Peer-reviewed version available at Metals 2017, 7, 416; doi:10.3390/met7100416

Article

Effect of Y Addition on the Semi-Solid Microstructure Evolution and the Coarsening Kinetics of SIMA AZ80 Magnesium Alloy

Qi Tang [1], Hao Sun [1], Mingyang Zhou [1] and Gaofeng Quan [1,*]

[1] Key Laboratory of Advanced Technologies of Materials, Ministry of Education, School of Material Science and Engineering, Southwest Jiaotong University, Chengdu 610031, China; tangqi@my.swjtu.edu.cn (Q.T.); 663116697@qq.com (H.S.); 1548454043@qq.com (M.Y.)

* Correspondence: quangf@swjtu.cn; Tel.: +86-139-8006-6985

Abstract: Semi-solid feedstock of AZ80 magnesium alloy modified by [trace] rare-earth Y element (0, 0.2, 0.4, 0.8 wt.%) were fabricated by [strain-induced melting activation] (SIMA) in the form of extrusion and partial remelting. The effect of Y addition on the microstructure evolution of [the] extruded and [isothermally heat] treated alloy was observed by [using an] optical microscope (OM), scanning electron microscope (SEM), X-ray diffraction (XRD) and quantitative analysis. The results show that the Y addition can refine the microstructure and make the β-$Mg_{17}Al_{12}$ phases [agglomerate]. During the subsequent isothermal treatment at 570℃, the average solid grain size, shape factor and liquid fractions increased with [the] prolonged soaking time. [The] smaller spheroidal solid grains and the larger shape factor were obtained [in the semi-solid microstructure] due to Y addition. The coalescence and Ostwald ripening mechanism operated the coarsening process [of solid grains] simultaneously. The coarsening rate constants of AZ80M1 (0.2 wt.% Y addition) of 164.22 $\mu m^3 s^{-1}$ was approximately four times less than the un-modified AZ80 alloy of 689.44 $\mu m^3 s^{-1}$. In contrast, the desirable semi-solid structure featured [with the] fine [and] well globular solid grains, [an] appropriate liquid fractions and shape factor was achieved in AZ80M1 alloy treated at 570℃ for 20-30 min.

Keywords: Mg-Al-Zn-Y magnesium alloy; SIMA; extrusion; semi-solid; microstructure evolution

1. Introduction

AZ80 is one of the most successful commercial magnesium alloys with the high-performance and high-strength, which has already been applied in the fields of aerospace, high-speed railway and automobiles in recent years [1-3]. However, magnesium alloy exhibits poor plastic deformation at room temperature owing to [the] hexagonal close-packed (HCP) structure with a limited number of slip systems [4,5]. [The] semi-solid forming (SSF) process as a new technology provides an effective approach to manufacture magnesium alloy components with complex shape and high mechanical properties [6,7]. Compared to [the] conventional forging or casting forming, the SSF process can effectively resolve the problem of metallurgical defects, such as over-burn, surface crack, porosity, macro-segregation and shrinkage [8-10]. Simultaneously, this process has a significant number of advantages, such as [the] small forming resistance, the extension of service life of forming die, production of the exact size and complex structural components, low production cost, and so on. These merits mainly derive from the fact that semi-solid alloys have a non-dendritic microstructure [11,12].

The major issue of the SSF process is the preparation of semisolid slurry with an ideal thixotropic microstructure with fine non-dendritic grains and an appropriated volume fraction of globular solid grains distributed uniformly within the liquid matrix [13]. The mechanical or electromagnetic stirring processes, semi-solid isothermal heat treatment (SSIT) and strain-induced melting activation (SIMA) method are the most common routes to produce semisolid slurry. [Compared to another two

methods], the SIMA process has high production efficiency and low equipment costs. This process mainly includes two steps[, namely,] cold or hot deformation and subsequent partial remelting in the semi-solid [temperature] range. It was reported from the previous literature that more spherical structure in AZ91D alloy semisolid slurry was obtained by the compression pre-deformed process as SIMA process [14]. Many researches also introduced severe plastic deformation (SPD) to be another effective SIMA approach for producing the semi-solid feedstock. Jiang et al. [15] investigated AZ61 magnesium alloy pre-deformed by equal channel angular extrusion (ECAE) before remelting activation. The results showed that [the] high-quality semisolid billets with fine and spherical solid particles can be [successfully] prepared by isothermally treating the ECAE-processed alloy. [Besides], repetitive upsetting-extrusion (RUE) was employed by Xu et al. [16] as the SIMA process [to] AZ91D magnesium alloy; it was found that the subsequent semi-solid feedstock with an ideal structure containing highly spherical and homogeneous solid grains. However, these [methods] are hard to apply in industrial production due to complex operations. The extrusion process is a promising and easy controlled method to obtain fine grains. And the coarse second phases with lower melting point in original microstructure can be effectively crushed. This may hasten the evolution of globular structure during [the] SSIT route, resulting in the high-quality semi-solid feedstock with more spherical and smaller solid grains [3,17].

The rare-earth elements (RE), such as neodymium (Nd), gadolinium (Gd) and yttrium (Y) are frequently added to magnesium alloy to enhance mechanical properties or corrosion behavior remarkably [18-20]. By comparison, Y is a light and [one of] the most effective RE element to improve mechanical properties of magnesium alloys, especially [for] the [mechanical properties at] elevated temperature owing to [its] considerable amount of solubility in Mg alloys [21]. Therefore, this research is aiming [at applying] the extrusion process as the SIMA approach to trace Y added AZ80 magnesium alloy. Microstructure evolution of extruded alloys in solid state and partial remelting state are investigated. In addition, the effect Y addition on [the] coarsening kinetics of deformed AZ80 alloy during the isothermal treatment in the semi-solid range [was] examined.

2. Materials and Methods

Table 1. Chemical composition of experimental alloys (wt.%).

Alloy		Mg	Al	Zn	Y
AZ80	[1]	Bal.	8.0	0.5	0
	[2]	Bal.	8.701	0.491	0
AZ80M1	[1]	Bal.	8.0	0.5	0.2
	[2]	Bal.	8.384	0.508	0.242
AZ80M2	[1]	Bal.	8.0	0.5	0.4
	[2]	Bal.	8.467	0.528	0.437
AZ80M3	[1]	Bal.	8.0	0.5	0.8
	[2]	Bal.	7.716	0.480	0.829

[1] nominal composition; [2] real composition

Four different types of materials used in this study based on AZ80 (Mg-8 wt.% Al-0.5 wt.% Zn) alloy. Inductively Coupled Plasma-Atomic Emission Spectrometer (ICP-AES) was used to examine the chemical composition, and the results [are] listed in Table 1. The pure magnesium (99.9 wt.%), pure aluminum (99.9 wt.%), pure zinc (99.9 wt.%), and Mg-30 wt.% Y master alloy were melted in electric resistance furnace under protected by CO_2+2 vol.% SF_6 mixed gas. The molten alloy was held at 720℃ for 40 min to ensure that yttrium was completely dissolved and then [smoothly] poured into [the] steel mould with a diameter of 95 mm. Subsequently, the billets were homogenized at 420°C for 12 h to eliminate [the] dendritic crystal structure. Then these billets were machined into columnar bars with a diameter of 90 mm. Prior to extrusion, the ingots and extrusion die were preheated to 350°C and maintained for 1 h. The oil-based graphite lubricant was used to reduce friction between

the die and ingot. Finally, the rods with a diameter of 16 mm were extruded at a speed of 15 mm s^{-1} with an extrusion ratio of about 32:1.

The [extrusion bars] were machined into [the] samples with a diameter of 10 mm and a height of 10 mm. These cylindrical samples were reheated to 570°C, with an accuracy of ± 2°C, [and maintained] for 5, 10, 20, 30 [minutes]. [Then] the samples were quenched in water immediately [after the isothermal treatment].

Microstructure of [the] extruded and semi-solid specimens was observed by [using] Zeiss Lab. A1 optical metallographic (OM) and Quanta FEG 250 scanning electron microscope (SEM) at a voltage of 20 kV. Samples for metallographic and SEM analysis were grounded, mechanically polished and etched in a solution of 1 g oxalic acid, 1 ml acetic acid, 1 ml nitric acid and 150 ml distilled water. The phase composition of [the] as-extruded alloys was identified by X-ray diffraction (XRD) analysis using Panalytical X'Pert Pro with Cu Kα1 radiation (λ=0.154 nm) [with] the scanning angle range from 20 to 80 degree, and the reflecting surface was perpendicular to the extrusion direction. The average grain size was determined by linear intercept method at least three pictures blindly selected and widely separate fields. Quantitative analysis [of] the micrographs of the specimens in the semi-solid state were carried out [using] by Image-Pro Plus software and the statistical results of solid fraction, shape factor were determined by three OM images. The shape factor of solid particles was calculated by the following equation [22]:

$$F_s=\frac{1}{n}\sum_{n=1}^{n}\frac{4\pi A}{P^2} \quad (1)$$

where F_s is the shape factor; n is the number of solid particles; A is the area of solid particles; P is the perimeter of solid particles.

3. Results and Discussion

3.1. Microstructure of [the] as-extruded alloy

Figure 1 shows the microstructures of [the] as-extruded AZ80 magnesium alloy with different Y contents on the cross section perpendicular to the extrusion direction (ED). It can be seen that Y had a remarkable effect on grain refinement. Figure 1a shows the as-extruded AZ80 without Y addition, the microstructure consists of equiaxed grains, and the average grain size is about 23.63 ± 2.52 μm. As well known, the dynamically recrystallized (DRX) behavior is the dominant mechanism for refining α-Mg matrix grains during [the] hot extrusion process [23]. Some new fine grains were formed at the original grain boundaries to form a typical necklace structures. As the Y contents increased to 0.2 wt.%, the fine grains (~15.94 ± 0.98 μm) were obtained, but it was heterogeneous, and some coarse ones (~22.54μm) can also be found in Figure 1b. When the addition of Y further increased to 0.4 and 0.8 wt.%, as was observed in Figure 1c and 1d, the bimodal microstructure was more obvious, which [consist of] relatively coarse DRX grains and fine DRX grains. However, the average grain sizes changed a little, corresponding to 9.74 ± 0.68 μm, 9.31 ± 0.34 μm approximately. The XRD pattern of [the] as-extruded AZ80 magnesium alloy with different amount of Y addition is shown in Figure 2. Three kinds of phases can be detected in these alloys, which are α-Mg, β-$Mg_{17}Al_{12}$ and Al_2Y, respectively.

Peer-reviewed version available at Metals 2017, 7, 416; doi:10.3390/met7100416

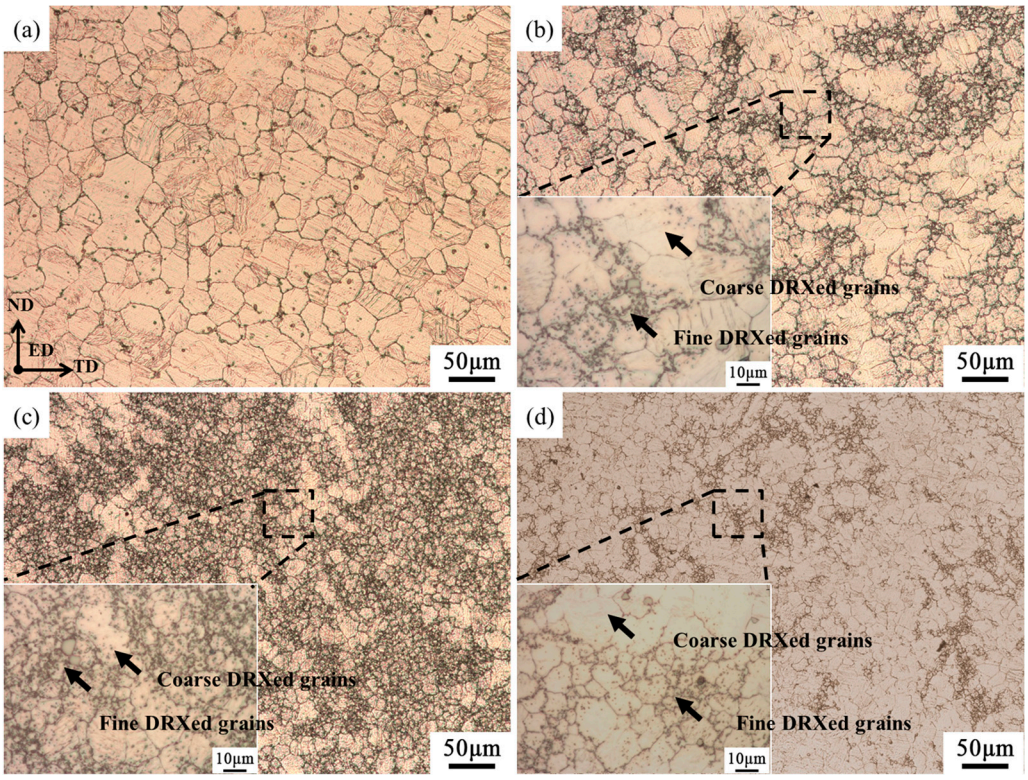

Figure 1. Microstructure of [the] extruded alloys: (**a**) AZ80; (**b**) AZ80M1; (**c**) AZ80M2; (**d**) AZ80M3.

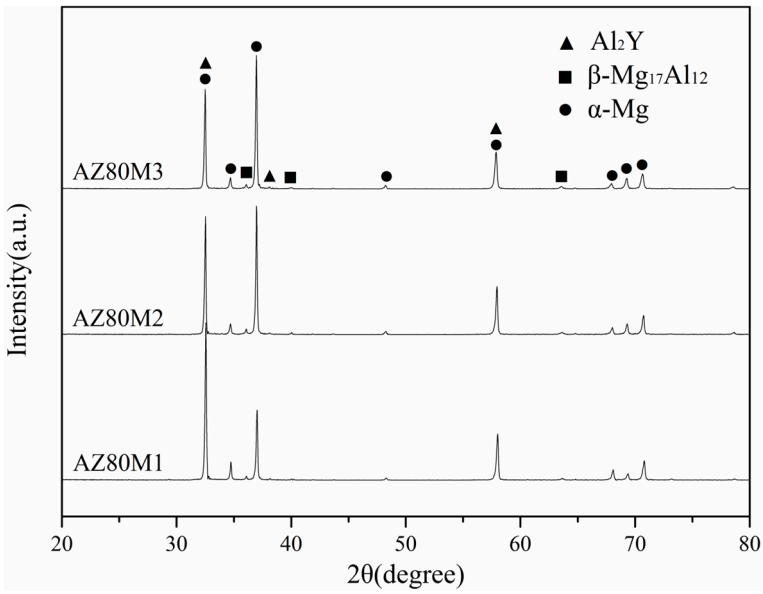

Figure 2. XRD patterns of AZ80 magnesium alloys with different Y contents

The β-$Mg_{17}Al_{12}$ and Al_2Y phases of [the] as-extruded AZ80 magnesium alloy with different addition Y are shown in Figure 3. As can be observed in Figure 3a, the AZ80 magnesium alloy only consist of α-Mg matrix and β-$Mg_{17}Al_{12}$ (marked with the red arrows). Compared to the alloy containing Y (seen from Figure 3b-3d), the β-$Mg_{17}Al_{12}$ were relatively larger and the size was between 1.8 μm and 2.5 μm assumably, which were mainly distributed evenly in the α-Mg matrix as semi-continuous network along the grain boundaries or dispersive particles within the α-Mg matrix. After the addition of Y, as shown in Figure 3b-3d, the network β-$Mg_{17}Al_{12}$ phases decreased, and a large amount of them transformed into more tiny granulous precipitates [with] the mean size [less than] 1.5 μm. Meanwhile, the irregular and blocky Al_2Y precipitates appeared, which was about 10 times

[larger] than β-$Mg_{17}Al_{12}$ particles (marked with yellow arrows). It was noteworthy that lots of fine granulous β-$Mg_{17}Al_{12}$ particles tended to agglomerate due to the dynamic precipitation process from the supersaturated α-Mg matrix, as represented in Figures 1b-1d and 3b-3d. The inhomogeneous distribution of β-$Mg_{17}Al_{12}$ phases increased with the addition of Y. Around the precipitation [agglomeration] regions, a large number of newly formed DRX grains can be found and the sub-micron precipitations were distributed more wildly at the boundaries of DRX grains. This is consistent with the findings of Guo et.al. [2], Huang et.al. [24], and Zhu et al. [25] for the investigation of [the] large strain hot rolling processed Mg-8Al alloy sheets, extrusion processed AZX912 alloy and multi-directional forging (MDF) processed AZ80 alloy, respectively. They all observed the dynamic precipitation, and eventually [the granular and inhomogeneous distribution β-$Mg_{17}Al_{12}$ phase caused] the formation of the coarse-grain zones and fine-grain zones. These phenomena can be attributed to the following two main reasons: (i) the fine β-$Mg_{17}Al_{12}$ particles may assist the particle stimulating nucleation (PSN) mechanism [26] to induce [more] nucleation of α-Mg grains at the interfaces of particles; (ii) these refinement particles could inhibit and suppress the growth of newly formed DRX grains during hot deformation process because the β-$Mg_{17}Al_{12}$ phases mainly precipitated at grain boundaries, in other word, these boundaries were pinned by these phases, resulting in difficult [migration].

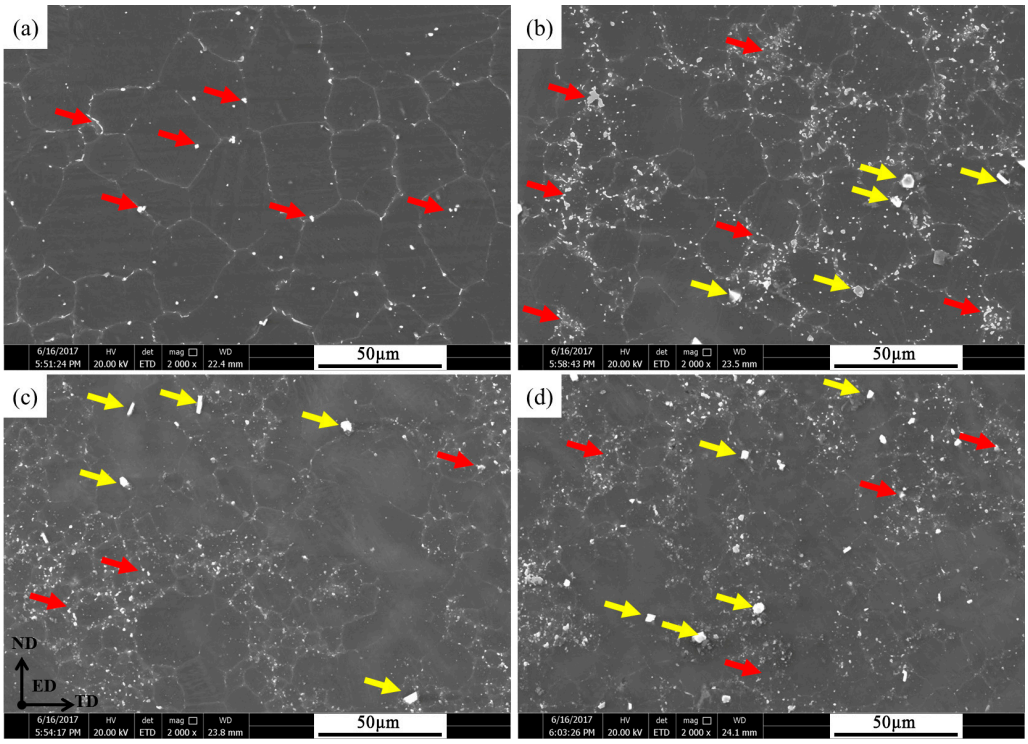

Figure 3. SEM images of [the] as-extruded alloys: (**a**) AZ80; (**b**) AZ80M1; (**c**) AZ80M2; (**d**) AZ80M3. (β-$Mg_{17}Al_{12}$ phase marked with the red arrow; Al_2Y phase marked with the yellow arrow)

3.2. Effect of Y addition on the microstructure evolution during isothermal treatment

Figures 4-7 illustrate the microstructure evolution of [the] as-extruded AZ80, AZ80M1, AZ80M2 and AZ80M3 alloy after soaking at 570℃ for different times, respectively. Compared with AZ80 alloy, it was clarified that the Y added samples have a vast number of spheroidal solid grains, and [the] sizes [of] intragranular liquid [droplets] increased obviously as the Y addition [increased] and the isothermal soaking time [prolonged] from 5 min to 30 min. Moreover, the size of globular solid particles and liquid fraction increased as well. Concerning the micrographs in Figure 4, the solid particles with polygonous boundaries distributed unevenly in the semi-solid slurry and more fine and dense liquid droplets were formed within α-Mg grains. Meanwhile, some smaller solid particles were discovered between the adjacent larger solid crystals. It was noteworthy that a quite

inhomogeneous microstructure appeared in all [the] three RE added alloys when [the] isothermal [treatment was conducted] at 570℃ for 5 min (as indicated by red arrows in Figure 4b, 4c and 4d) because liquid phase was not infiltrated along the boundaries. This was similar to the investigation of [the] microstructure evolution during reheating [the] extruded Mg-Al-Zn alloy by Kleiner et al. [17]. As well known, the initial liquid phase mainly originated from [the] melting of some low-melting point precipitates, which occurred at the triple points of grain boundaries firstly. With the partial remelting further developing, the liquid phases started infiltrating along the grain boundaries and the intragranular liquid droplets also appeared. Combined with the phase distribution depicted in Figure 1 and Figure 3, the varying degrees of β-$Mg_{17}Al_{12}$ precipitation agglomeration appeared in the Y added alloys. This phenomenon may lead to the non-uniform [distribution of] Al in the matrix, [leading to] the formation of Al-rich regions and Al-poor regions. According to the Mg-Al binary alloy phase diagram [27], the solidus temperature decreased with increasing Al contents below 12 wt.%. So the remelting behavior may start at Al-rich regions and no grains boundaries were wetted in the Al-poor areas when the temperature was below the solidus temperature, which [could] account for the inhomogeneous remelting microstructure at grain boundaries illustrated in Figures 4b, 4c and 4d. In summary, the segregation of β-$Mg_{17}Al_{12}$ phases evidently influenced the semi-solid microstructure in the early stage of [partial] remelting.

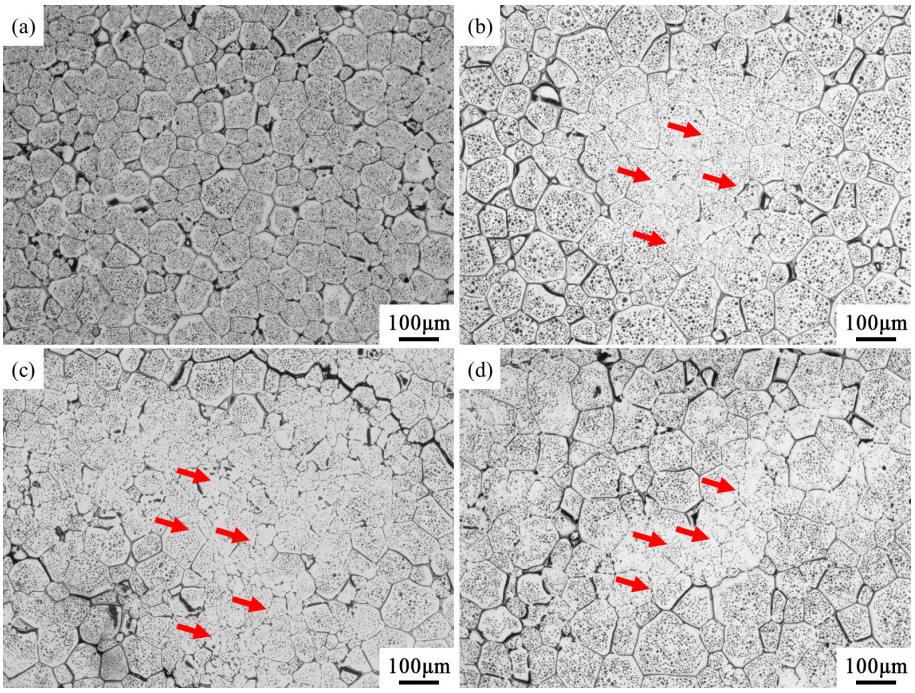

Figure 4. Microstructure evolution of alloys isothermally treated at 570℃ holding for 5 min: (**a**) AZ80; (**b**) AZ80M1; (**c**) AZ80M2 and (**d**) AZ80M3.

Continue to increase the holding time to 10 min, as shown in Figure 5, the size of the majority of solid particles became bigger in all alloys as a result of the Oswald ripening mechanism or the coalescence of two adjacent solid grains, and the former was considered as the dominant coarsening mechanism generally [11,28]. Furthermore, the liquid droplets within solid crystals transformed to [the] suborbicular liquid pools [with] the size from 10 to 20 μm, and the liquid films between solid α-Mg also became thicker in AZ80 alloy modified by Y element. However, some inhomogeneous microstructure regions were also found in AZ80M2 (as indicated by red arrows) in Figure 5c. This was attributed to severe β-$Mg_{17}Al_{12}$ phase agglomeration in the extruded corresponding alloy in Figure 1c.

Peer-reviewed version available at Metals 2017, 7, 416; doi:10.3390/met7100416

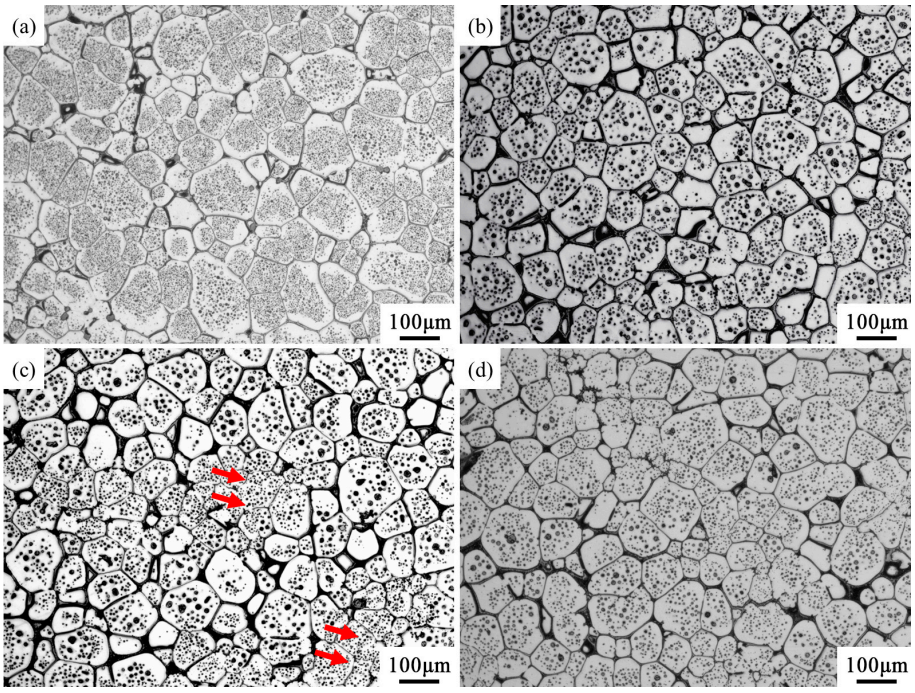

Figure 5. Microstructure evolution of alloys isothermally treated at 570℃ holding for 10 min: (**a**) AZ80; (**b**) AZ80M1; (**c**) AZ80M2 and (**d**) AZ80M3.

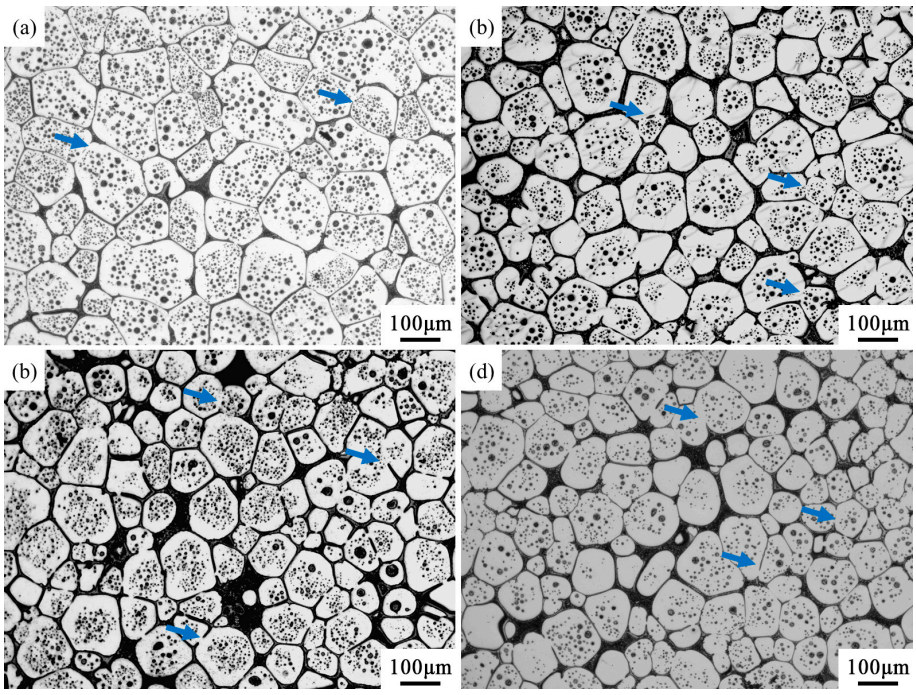

Figure 6. Microstructure evolution of alloys isothermally treated at 570℃ holding for 20 min: (**a**) AZ80**;** (**b**) AZ80M1; (**c**) AZ80M2 and (**d**) AZ80M3.

Further prolonging the isothermal time to 20 min, as seen in Figure 6, the average grain size and globularity of solid particles increased distinctly. Meanwhile, the liquid films between solid particles became much thicker and more continuous after Y addition. However, the decrease in the number of intragranular liquid droplets was exhibited. A few solid particles lower than the average grain size were also existed, which can be attributed to the Ostwald ripening mechanism [29]. This process was that the diameter of [the] bigger grains increased at expense of the smaller ones during the partial remelting. It can be seen that some adjacent solid grains were interconnected to form a bigger one, as

Peer-reviewed version available at Metals 2017, 7, 416; doi:10.3390/met7100416

indicated by blue arrows in Figure 6. This was also demonstrated by Xu et al. [16] and Chen et al. [30] for the research on the semi-solid microstructure evolution of RUE-formed and ECPA-formed AZ91D alloy, and they suggested [that] the Ostwald ripening mechanism and the coalescence of solid particles operated simultaneously and independently for the grains coarsening.

When the soaking time extended to 30 min (Figure 7), it can be observed that the size and sphericity of solid α-Mg were further increased. Moreover, a small number of larger and more globular liquid pools gathered in the core region of solid particles in all alloys to minimize the system's total surface area according to the energy theory [16,20]. The higher liquid fraction is, the smaller probability of [the] coalescence of solid grains is. Therefore, the Ostwald ripening mechanism became the dominant [mechanism] for grain growth after a long time holding at 570℃ owing to the more atoms diffusion in [the] melted regions along liquid phase. In contrast, AZ80 with addition of 0.2 wt.% Y obtained the desired structure with finer solid grain size and uniform in the shape of α-Mg and thickness of liquid films.

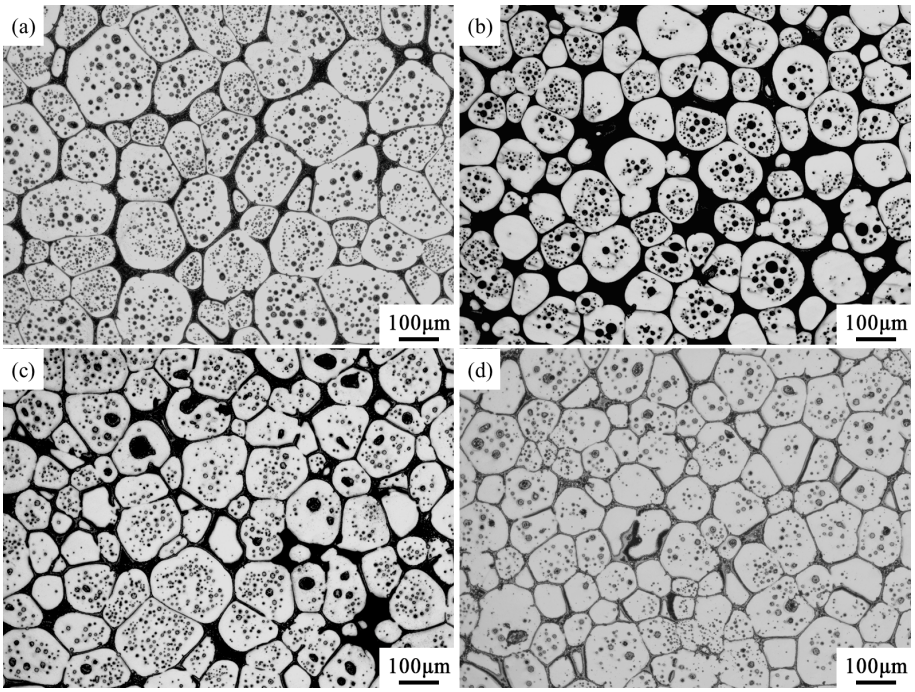

Figure 7. Microstructure evolution of alloys isothermally treated at 570℃ holding for 30 min: (**a**) AZ80; (**b**) AZ80M1; (**c**) AZ80M2 and (**d**) AZ80M3.

3.3. Shape factor, average solid grain size and solid fraction of the alloys

[The] shape factor and average grain size of solid particles are shown in Figure 8 and Figure 9, respectively. As treated for 5 min, 10 min, 20 min and 30 min, both of [the] shape factor and average solid grain size gradually [increased] during [the isothermal] holding at 570℃. These results indicated that the coarsening and spheroidization were introduced by the prolonging soaking time. However, the average solid grain size of the Y-containing alloys showed a little bigger than the AZ80 alloy when the time was no more than 10 min, which could be attributed to [the] β-$Mg_{17}Al_{12}$ phase segregation and resulting in the grains without clear boundaries during the initial stage of isothermal treatment. Furthermore, not only [the] shape factor but also [the] average solid grain size in AZ80M alloy was lower than the unmodified one. It can be concluded that the rare-earth Y element was valid to refine the microstructure of semi-solid magnesium alloy. In other words, the growth of solid particles has been excessively restricted by adding [the] rare earth Y element.

Preprints (www.preprints.org) | NOT PEER-REVIEWED | Posted: 15 September 2017 doi:10.20944/preprints201709.0067.v1

Peer-reviewed version available at Metals 2017, 7, 416; doi:10.3390/met7100416

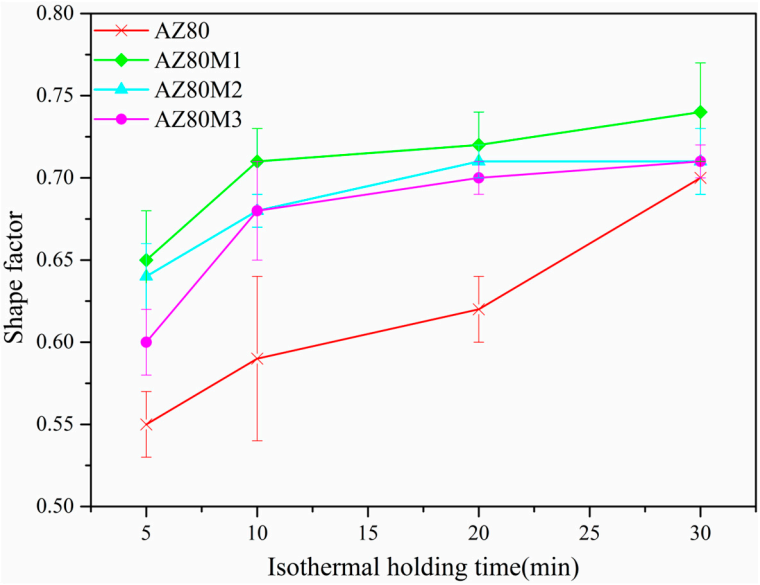

239

240 **Figure 8.** Effect of Y addition on the shape factor at 570℃ for different isothermal holding time

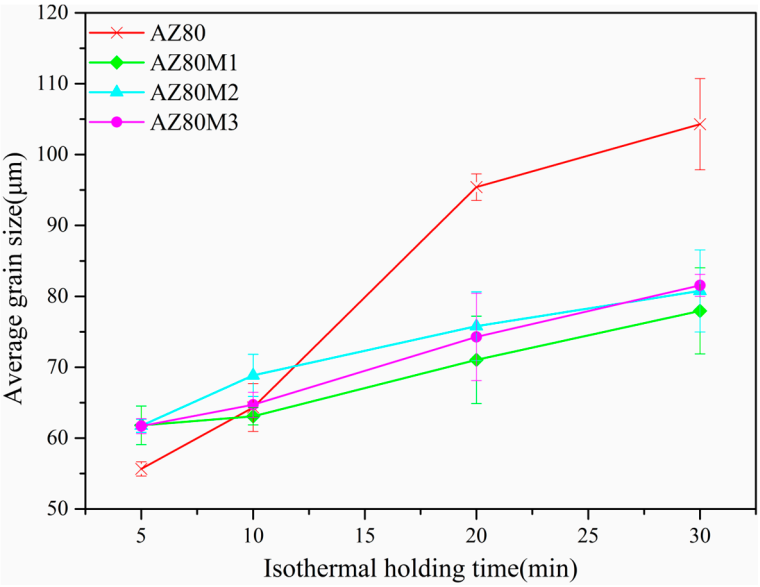

241

242 **Figure 9.** Effect of Y addition on the average solid grain size at 570℃ for different isothermal
243 holding time

244 **Table 2.** Solid fraction of [the] experimental alloys at 570℃ for various isothermal time

Alloy	5min	10min	20min	30min
AZ80	0.81	0.75	0.70	0.69
AZ80M1	0.80	0.74	0.72	0.71
AZ80M2	0.77	0.72	0.69	0.69
AZ80M3	0.80	0.75	0.69	0.69

245 The solid fraction of the alloys is presented in Table 2. The solid volume fraction varied in the
246 range from 0.69 to 0.81 and increased with the [prolonging] isothermal soaking time from 5 min to
247 30 min. It was revealed that the semi-solid slurry with a high solid fraction between 0.75 and 0.8
248 owned the better [thixotropic] behavior [6,22]. Moreover, the forming defects such as porosity,

inclusions or shrinkage could be visibly prevented in [the] high solid fraction semi-solid feedstock during the forming process. However, the lower spheroidization of solid particles was unfavorable for the thixotropic behavior [8,14]. Therefore, it is expected that the AZ80 modified by 0.2 wt.% Y may be deemed as the optimal semi-solid slurry to achieve the thixotropic applications on the basis of the smaller solid grain size, the larger shape factor and [an] appropriate solid fraction.

3.4. Spheroidization and coarsening mechanisms of semi-solid microstructure

The Oswald ripening governed by the Gibbs-Thompson effect have been [widely] reported by many researchers [5,31], which altered the solute atomic concentration at the solid particles interface depending on the curvature of the solid-liquid interface, according to [the] Gibbs-Thompson formula expressed by the following expression:

$$C_\alpha(r)=C_\alpha(\infty)\, exp\left(\frac{2\sigma V_B}{k_B T r}\right) \quad (2)$$

where $C_\alpha(r)$ is the atom concentration at the site with a curvature radius r; $C\alpha(\infty)$ is the atom concentration at a flat interface; σ is the surface tension; V_B is the volume of atom; T is the temperature and k_B is the shape coefficient.

According to Eq. (2), the smaller the curvature radius r is, the higher the atom concentration will be. Generally, the different positions of solid particles have [a] different curvature radius due to an irregular shape, which causing a gradient of atom concentration between these areas. During the isothermal soaking treatment, the atoms will diffuse from [the] relatively larger curvature where the atom concentration is high to the flat interface where the atom concentration is low, so the balance of atom concentration is broken. Therefore, the sites with larger curvature would be dissolved to keep the balance of atom concentration. Then the suborbicular or spherical solid α-Mg was formed.

Subsequently, the Gibbs free energy (ΔG) of single grain under a function of the interface curvature and the solid-liquid interfacial energy can be expressed by the following expression:

$$\Delta G=2\gamma\frac{\Delta V}{r} \quad (3)$$

where r and γ are the average curvature radius and interfacial energy of the solid-liquid interface in the semisolid slurry, respectively; ΔV is the variation molar volume.

The Gibbs free energy (ΔG) could serve as the driving force for the grains growth [11]. The solid α-Mg particles adjusted by the Oswald ripening mechanism could be considered having the similar curvature radius and molar volume owing to [the] suborbicular or spherical shape. Previous literatures [20,30,32] have been concluded that the rare earth elements was surface-active element and they could decrease the surface energy of the alloys melt, which resulting in reducing the solid-liquid interfacial energy. Therefore, the value of ΔG decreased due to the reduction of the solid-liquid interfacial energy by adding Y element. Moreover, the inadequate and discontinuous liquid films occurred in the initial stage of partial remelting. It was reported that two solid α-Mg merged only when the interfacial energy between the solid and liquid phase (γ_{sl}) was bigger than the interfacial energy between the solid particles (γ_{ss}) [33]. However, the decreasing of γ_{sl} caused by Y addition has been difficult to satisfy the condition of $\gamma_{sl} > \gamma_{ss}$. So the coalescence of the solid α-Mg was sharply hindered. Therefore, it can be concluded the comprehensive effect of the reduction of Gibbs free energy (ΔG) and the decreasing probability of coalescence of adjacent solid α-Mg particles make the spherical structure with relatively finer grain size in the semi-solid slurry of AZ80 alloy modified by RE element.

3.5. Coarsening kinetics of the alloys

During the isothermal soaking process, the coarsening of solid particles is mainly controlled by the Ostwald ripening mechanism. The coarsening kinetics can be described by the classical Lifshitz-Slyozov-Wagner (LSW) equation [34]:

$$D^n-D_0^n=kt \quad (4)$$

Peer-reviewed version available at Metals 2017, 7, 416; doi:10.3390/met7100416

where D is the final average grain size; D_0 is [the] initial average grain size; t is the isothermal holding time; k is the coarsening rate constant; n is the power exponent. It was believed that [the] n value of 3 is suitable for investigating the volume diffusion-controlled coarsening in the semi-solid state during partial remelting [9,12].

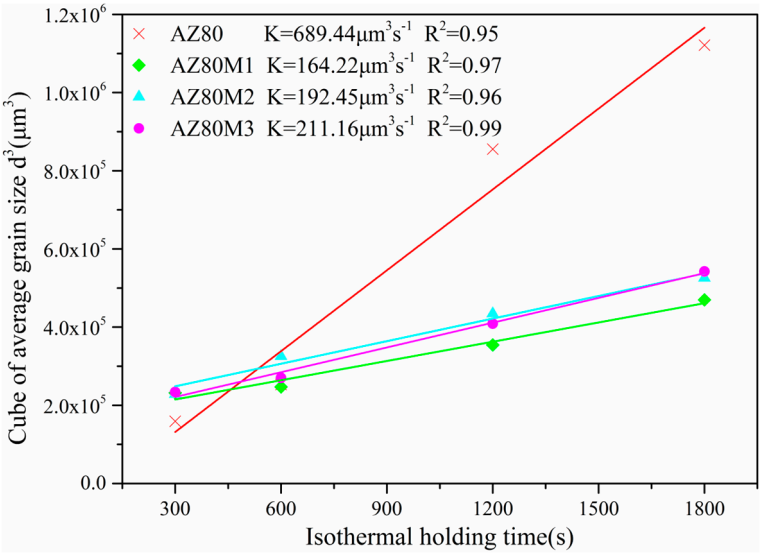

Figure 10. Effect of Y addition on the coarsening kinetics at 570℃

The cube of experimental results of [the] average solid grain sizes as a function of the isothermal holding time for [the] as-extruded AZ80 containing different Y contents at 570℃ is plotted in Figure 10. The value of D_0 was the average grain size when the soaking time was 5 min in this paper. It can be confirmed that the coarsening kinetics of all the four kinds of alloys during the isothermal heating had the best correlation with the Eq. (4). This was determined by the regression coefficient (R^2) of [the] fitted straight lines all close to 1. The values of k obtained from the slope of fitted lines in Figure 10 were 689.44 $\mu m^3 s^{-1}$, 164.22 $\mu m^3 s^{-1}$, 192.45 $\mu m^3 s^{-1}$ and 211.16 $\mu m^3 s^{-1}$ in AZ80, AZ80M1, AZ80M2 and AZ80M3 alloy respectively. It was shown that the coarsening rate was significantly slower by [adding] Y element due to the reduction of the solid-liquid interfacial energy. In addition, it was clearly noticed that the minimum k value achieved in [the extruded] AZ80M1, [which] was approximately 4.2 times less than the maximum one in the non-modified AZ80 alloy. However, with the further adding Y [up] to 0.4 and 0.8 wt.%, the slightly increased k value was found. This rising may be attributed to the change of liquid phase fraction, as shown in Table 2. Usually, the particle growth also depends on diffusion or flow of solute atoms between [the] solid particles of different size. The experimental results were similar to the results observed by Ferrante et al. [35] and Manson-Whitton et al. [36]. They reported that either the compressed or the spray formed Al-4Cu(wt.%), the increase in the quantity of liquid fraction could accelerate the coarsening rate of solid particles during [the] isothermal treatment. Because the liquid could provide a much faster diffusion path than the solid. In case the continuous liquid path was formed around the spherical solid α-Mg, the coarsening effect can [be accelerated]. Considering mentioned above, the AZ80M1 possesses the superior slow coarsening rate, which could serve as the best semi-solid feedstock for [the thixotropic behavior].

4. Conclusions

In this paper, the semi-solid feedstock of AZ80 magnesium alloy (Mg-8 wt.% Al-0.5 wt.% Zn) modified by trace rare-earth Y element (0, 0.2, 0.4, 0.8 wt.%) was prepared by the SIMA approach by employing the extrusion process. The microstructures evolution of [the] extruded and [isothermally] soaking treated alloys was investigated. And the main conclusions can be summarized as follows:

(1) The rare earth element Y had a remarkable effect on the refinement [of] microstructure of AZ80 magnesium alloy during the extrusion process. However, the agglomeration of β-$Mg_{17}Al_{12}$

phases appeared in the Y added alloys, which causing a quite inhomogeneous microstructure at the initial stage of partial remelting.

(2) During the isothermal treatment at 570℃ for different soaking time, the Y added alloys had more spheroidal and fine solid grains. The spheroidization of solid grains can be simply explained using the Gibbs-Thompson formula.

(3) Both of the coalescence and Ostwald ripening mechanism affected the coarsening of microstructure in the semi-solid slurry. The coarsening rate constants of 689.44 $\mu m^3 s^{-1}$, 164.22 $\mu m^3 s^{-1}$, 192.45 $\mu m^3 s^{-1}$ and 211.16 $\mu m^3 s^{-1}$ were [obtained] in AZ80, AZ80M1, AZ80M2 and AZ80M3 alloy soaked at 570℃, respectively. It can be seen that the coarsening rate of solid particles decreased significantly by the addition of Y element.

(4) The 0.2 wt.% Y added AZ80 alloy subjected to [the] extrusion and subsequent isothermal treatment at 570℃ for 20-30 min was considered as the optimal semi-solid feedstock, which contained the greater shape factor, the homogeneous [solid particles] and [an] appropriate solid fraction.

Acknowledgments: The present research was supported by the 2017 key development project of Sichuan Province (No: 2017GZ0399).

Author Contributions: Gaofeng Quan and Qi Tang conceived and designed the experiment; Qi Tang, Mingyang Zhou and Hao Sun performed the experiment; Qi Tang and Hao Sun analyzed the data; Qi Tang wrote the paper; and Qi Tang, Hao Sun and Mingyang Zhou revised the paper.

Conflicts of Interest: The authors declare no conflict of interest.

References

1. Huang, X.; Suzuki, K.; Saito, N. Microstructure and mechanical properties of AZ80 magnesium alloy sheet processed by differential speed rolling[J]. *Mater. Sci. Eng. A* **2009**, *508*, 226-233. [CrossRef]
2. Guo, F.; Zhang, D.F; Yang, X.S; Jiang, L.Y; Pan, F.S. Strain-induced dynamic precipitation of $Mg_{17}Al_{12}$ phases in Mg-8Al alloys sheets rolled at 748 K[J]. *Mater. Sci. Eng. A* **2015**, *636*, 516-521. [CrossRef]
3. Jiang, W.Y.; Chen, T.; Wang, L.P.; Feng, Y.C.; Zhu, Y.; Wang, K.F.; Luo, J.P.; Zhang, S.W. Microstructure in the semi-solid state and mechanical properties of AZ80 magnesium alloy reheated from the as-cast and extruded states[J]. *Acta Metall. Sinica*. **2013**, *26*, 473-482. [CrossRef]
4. Staroselsky, A.; Anand, L. A constitutive model for hcp materials deforming by slip and twinning : application to magnesium alloy AZ31B[J]. *Inter. J. Plasticity*, 2003, *19*, 1843-1864. [CrossRef]
5. Wang, J.G.; Lin, H.Q.; Wang, H.Y.; Jiang, Q.C. Effects of different processing parameters on the semisolid microstructure of the AZ91D alloy during partial remelting. *J. Alloys Compd*. **2008**, *466*, 98-105. [CrossRef]
6. Mansoor, B.; Mukherjee, S.; Ghosh, A. Microstructure and porosity in thixomolded Mg alloys and minimizing adverse effects on formability[J]. *Mater. Sci. Eng. A* **2009**, *512*, 10-18. [CrossRef]
7. Chen, D.L.; Sadayappan, K.; Patel, H.A.; Bhole, S.D. Microstructure and tensile properties of thixomolded magnesium alloys[J]. *J. Alloys Compd.* **2010**, *496*, 140-148. [CrossRef]
8. Wang, C.P.; Tang, Z.J.; Mei, H.S.; Wang, L.; Li, R.Q.; Li, D.F. Formation of spheroidal microstructure in semi-solid state and thixoforming of 7075 high strength aluminum alloy[J]. *Rare Metals*. **2015**, *34*, 710-716. [CrossRef]
9. Tzimas E, Zavaliangos A. A comparative characterization of near-equiaxed microstructures as produced by spray casting, magnetohydrodynamic casting and the stress induced, melt activated process[J]. *Mater. Sci. Eng. A* **2000**, *289*, 217-227. [CrossRef]
10. Wang, C.L.; Chen A.; Zhang L, Liu, W.C; Wu, G.H; Ding, W.J. Preparation of an Mg-Gd-Zn alloy semisolid slurry by low frequency electro-magnetic stirring[J]. *Mater. Des*. **2015**, *84*, 53-63. [CrossRef]
11. Binesh, B.; Aghaie-Khafri, M. Phase Evolution and Mechanical Behavior of the Semi-Solid SIMA Processed 7075 Aluminum Alloy[J]. *Metals*. **2016**, *6*, 42. [CrossRef]
12. Haghdadi, N.; Zarei-Hanzaki, A.; Heshmati-Manesh, S.; Abedi, H.R.; Hassas-Irani, S.B. The semisolid microstructural evolution of a severely deformed A356 aluminum alloy[J]. *Mater. Des*. **2013**, *49*, 878-887. [CrossRef]
13. Binesh, B.; Aghaie-Khafri, M. Microstructure and texture characterization of 7075 Al alloy during the SIMA process[J]. *Mater. Charact*. **2015**, *106*, 390-403. [CrossRef]

14. Zhang, Q.Q.; Cao, Z.Y.; Zhang, Y.F; Su, G.H.; Liu, Y.B. Effect of compression ratio on the microstructure evolution of semisolid AZ91D alloy[J]. *J. Mater. Process. Technol*. **2007**, *184*, 195-200. [CrossRef]
15. Jiang, J.F.; Lin, X.; Wang, Y. Jian-Jun, Q.U.; Luo, S.J. Microstructural evolution of AZ61 magnesium alloy predeformed by ECAE during semisolid isothermal treatment[J]. *Trans. Nonferrous Metals Soc. China* **2012**, *22*, 555-563. [CrossRef]
16. Xu, Y.; Hu, L.X; Jia, J.B, Xu, B. Microstructure evolution of a SIMA processed AZ91D magnesium alloy based on repetitive upsetting-extrusion (RUE) process[J]. *Mater. Character*. **2016**, *118*, 309-323. [CrossRef]
17. Kleiner, S.; Beffort, O.; Uggowitzer, P.J. Microstructure evolution during reheating of an extruded Mg-Al-Zn alloy into the semisolid state[J]. *Scr. Mater*. **2004**, *51*, 405-410. [CrossRef]
18. Liu, L.; Yuan, F.; Zhao, M.; Gao, C.; Feng, P.; Yang, Y.; Yang, S.; Shuai, C. Rare Earth Element Yttrium Modified Mg-Al-Zn Alloy: Microstructure, Degradation Properties and Hardness. *Mater*. **2017**, *10*, 477. [CrossRef]
19. Tekumalla, S.; Seetharaman, S.; Almajid, A.; Gupta, M. Mechanical Properties of Magnesium-Rare Earth Alloy Systems: A Review. *Metals*. **2015**, *5*, 1-39. [CrossRef]
20. Nami, B.; Shabestari, S.G.; Miresmaeili, S.M.; Razavi, H.; Mirdamadi, S. The effect of rare earth elements on the kinetics of the isothermal coarsening of the globular solid phase in semisolid AZ91 alloy produced via SIMA process[J]. *J. Alloys Compd*. **2010**, *489*, 570-575. [CrossRef]
21. Son, H.T.; Kim, Y.H.; Kim, T.S.; Lee, S.H. Mechanical Properties and Fracture Behaviors of the As-Extruded Mg-5Al-3Ca Alloys Containing Yttrium at Elevated Temperature.[J]. *J. Nanoscien Nanotechnol*. **2016**, *16*, 1806. [CrossRef]
22. Chen, X.H.; Yan, H. Constitutive behavior of Al_2O_3np/Al7075 composites with a high solid fraction for thixoforming[J]. *J. Alloys Compd*. **2017**, *708*, 751-762. [CrossRef]
23. Cai, Z.; Chen, F.; Ma, F.; Guo, J. Dynamic recrystallization behavior and hot workability of AZ41M magnesium alloy during hot deformation[J]. *J. Alloys Compd*. **2016**, *670*, 55-63. [CrossRef]
24. Huang, X.; Chino, Y.; Yuasa, M.; Uedab, H.; Inoueb, M.; Kidoc, F.; Matsumotoc, T. Microstructure and mechanical properties of AZX912 magnesium alloy extruded at different temperatures[J]. *Mater. Sci. Eng. A* **2017**, *679*, 162-171. [CrossRef]
25. Zhu, Q.F.; Wang, G.S.; Zhang, E.G.; Liu, F.Z.; Zhang, Z.Q.; Cui, J.Z. Dynamic and Static Aging Precipitation of β-$Mg_{17}Al_{12}$ in the AZ80 Magnesium Alloy During Multi-directional Forging and Subsequent Aging[J]. *Acta Metall. Sinica*. **2017**, 1-8. [CrossRef]
26. Robson, J.D.; Henry, D.T.; Davis, B. Particle effects on recrystallization in magnesium-manganese alloys: Particle-stimulated nucleation[J]. *Acta Mater*. **2009**, *57*, 2739-2747. [CrossRef]
27. Mezbahulislam, M.; Mostafa, A.O.; Medraj, M. Essential Magnesium Alloys Binary Phase Diagrams and Their Thermochemical Data[J]. *J. Mater*. **2014**, *2014*, 33. [CrossRef]
28. Li, P.; Chen, T.; Zhang, S.; Guan, R. Research on Semisolid Microstructural Evolution of 2024 Aluminum Alloy Prepared by Powder Thixoforming[J]. *Metals*. **2015**, *5*, 547-564. [CrossRef]
29. Haghdadi, N.; Zarei-Hanzaki, A.; Heshmati-Manesh, S.; Abedi, H.R.; Hassas-Irani, S.B. The semisolid microstructural evolution of a severely deformed A356 aluminum alloy[J]. *Mater. Des*. **2013**, *49*, 878-887. [CrossRef]
30. Chen, T.J.; Ma, Y.; Li, Y.D.; Lu, G.X.; Hao, Y. Microstructural evolution of equal channel angular pressed AZ91D magnesium alloy during partial remelting[J]. *Mater. Sci. Tech*. **2013**, *26*, 1197-1206. [CrossRef]
31. Tzimas, E.; Zavaliangos, A. Evolution of near-equiaxed microstructure in the semisolid state[J]. *Mater. Sci. Eng. A* **2000**, *289*, 228-240. [CrossRef]
32. Nayyeri, M.J.; Khomamizadeh, F. Effect of RE elements on the microstructural evolution of as cast and SIMA processed Mg-4Al alloy[J]. *J. Alloys Compd*. **2012**, *509*, 1567-1572. [CrossRef]
33. Loué, W.R.; Suéry, M. Microstructural evolution during partial remelting of Al-Si7Mg alloys[J]. *Mater. Sci. Eng. A* **1995**, *203*, 1-13. [CrossRef]
34. Atkinson, H.V.; Liu, D. Microstructural coarsening of semi-solid aluminium alloys[J]. *Mater. Sci. Eng. A* **2008**, *496*, 439-446. [CrossRef]
35. Ferrante, M.; Freitas, E.D. Rheology and microstructural development of a Al-4wt.%Cu alloy in the semi-solid state[J]. *Mater. Sci. Eng. A* **1999**, *271*, 172-180. [CrossRef]
36. Manson-Whitton, E.D.; Stone, I.C.; Jones, J.R.; Grant, P.S.; Cantor, B. Isothermal grain coarsening of spray formed alloys in the semi-solid state[J]. *Acta Mater*. **2002**, *50*, 2517-2535. [CrossRef]